A novel K-means based Glaucoma Detection

J.Jaspin Jeni
PG Student
Department of ECE
Satyam College of Engineering
E-mail : jaspinjeni59@gmail.com

Abstract- Glaucoma is an irreversible chronic eye disease that leads to vision loss. As it can be slowed down through treatment, detecting the disease in time is important. However, many patients are unaware of the disease because it progresses slowly without easily noticeable symptoms. Currently, there is no effective method for low-cost population-based glaucoma detection or screening. Recent studies have shown that automated optic nerve head assessment from 2-D retinal fundus images is promising for low-cost glaucoma screening. In this paper, we propose a method for cup to disc ratio (CDR) assessment using 2-D retinal fundus images. In the proposed method, the optic disc is first segmented and reconstructed using a novel sparse is similarity constrained coding (SDC) approach which considers both the dissimilarity constraint and the sparsity constraint from a set of reference discs with known CDRs. The proposed method has been tested for CDR assessment in a database of 650 images with CDRs manually measured by trained professionals previously. The proposed method achieves good accuracy for glaucoma detection.

Keywords: **Cup to disc ratio (CDR), glaucoma screening, sparse dissimilarity-constrained coding (SDC).**

1 INTRODUCTION

Glaucoma is a chronic eye disease. It is the leading cause of irreversible blindness, and is predicted to affect around 80 million people by 2020 [1]. As the disease progresses silently without easily noticeable visual symptoms especially in the early stages, 50–90% of patients are unaware of the disease until it has reached its advanced stages [2]–[4]. Thus, glaucoma is also called the silent theft of sight. Although glaucoma cannot be cured currently, it can be slowed down through treatment. This makes the screening of people at high risk of glaucoma for timely detection very meaningful. Currently, the air-puff intraocular pressure (IOP) measurement, visual field test, and optic nerve head (ONH) assessment are often used in glaucoma assessment. However, the IOP measurement provides low accuracy in glaucoma detection and a visual field examination requires special equipment only present in specialized hospitals. Therefore, they are unsuitable for screening in the population. ONH assessment is more promising for glaucoma screening. It can be done by a trained professional. However, manual assessment is subjective, time consuming, and expensive. In recent years, automated algorithms for ONH assessment have received much attention. There is some research into automated cup to disc ratio (CDR) assessment from 3-D images such as stereo images [5] and optical coherence tomography images [6]–[8]. However, the cost of obtaining 3-D images is still high, which makes it inappropriate for low-cost large-scale screening [9]. The 2-D retinal fundus images can be acquired at much lower cost because such fundus cameras are widely available in hospitals, polyclinics, eye centers, and especially in optical shops. Therefore, there is little additional hardware cost to build a glaucoma screening program using existing fundus cameras.

1.1 Automated CDR Assessment

This paper is for automated CDR assessment from 2-D fundus images. One strategy for automatic ONH assessment is to use image level features for a binary classification between glaucomatous and healthy subjects [10]–[12]. In these methods, selection of features and classification strategy is difficult and challenging [9]. The other strategy is to follow clinical indicators. Many glaucoma risk factors can be considered, such as the vertical CDR [13], disc diameter [14], ISNT [15] rule, etc.

Early detection and treatment of retinal diseases are crucial to avoid preventable vision loss. Digital colour fundus (retinal) image (CFI) has emerged as a preferred imaging modality for large scale eye screening programs due to its noninvasive nature. The optic disk (OD) one of the main component of retina

(shown in fig 1(a)), is an important indicator for *glaucoma* which is one of the most common causes of blindness.

The intensity variations within the OD and its vicinity make OD boundary localisation challenging. The cup is primarily defined using 3D depth. Clinicians use high end imaging such as Heidelberg Retina Tomograph (HRT), Optical Coherence Tomography (OCT) to get 3D depth information. Detecting cup boundary from a CFI alone (without 3D depth information) is much more challenging task [1][2]. Much of prior work on quantification of OD appearance has mainly focused on OD boundary detection whereas handful attempts are made to detect cup boundary. However, detection of both boundaries is a fundamental requirement to estimate disk parameters and therefore to aid detection of glaucoma.

The CDR is computed as the ratio of the vertical cup diameter to the vertical disc diameter clinically. Many methods have been proposed for CDR assessment/computation from 2-D images. In [16], thresholding based on intensity is used. However, in many subjects from screening, the cup boundaries are not clear from intensity. The challenge is to correctly identify the vessel bends. Yin *et al.* developed an active shape model (ASM)-based approach by combining prior knowledge with contour deformation [17]. However, the contour deformation does not work well when the contrast between the cup and rim is weak. Cheng *et al.* proposed superpixel classification-based approach [18] by including features from superpixel level, which significantly improves the disc and cup detection. Very often, these methods rely on the contrast between the cup and the neuroretinal rim to find the cup boundary for CDR computation and can be challenging to use effectively when the contrast is weak. Recently, Xu *et al.* proposed a reconstruction or atlas-based method for cup estimation from the discs [19]. The method applies locality-constrained linear coding (LLC) [20] with _2-normGaussian distance regularization to reconstruct the disc from a set of reference images with known CDRs.
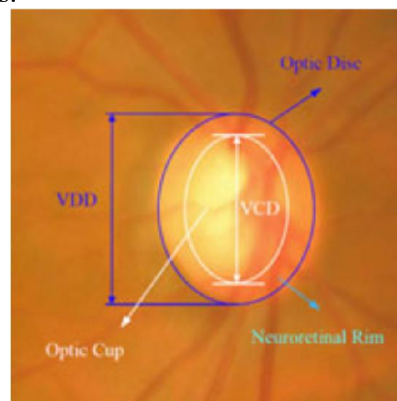
Figure 1.1: Structure of an optic disc: optic disc boundary (blue), optic cup (white), neuroretinal rim (cyan), CDR is computed as VCD/VDD.

It significantly reduces the CDR errors. However, the _2-norm Gaussian distance suffers from the blood vessels (BV) occlusion and other noise, which lead to a bias similar to the superpixel-based method [18]. This paper focuses on computing the CDR from the disc. Motivated from the observation that similar discs often have very similar CDRs and the fact that many discs do not have obvious boundary between neuroretinal rim and the optic cup, we propose a sparse dissimilarity-constrained coding (SDC) to estimate the CDR for a new disc image. In comparison with the LLC method [19] which uses the Gaussian distance, the proposed method computes the dissimilarities between the testing disc images and the reference disc images from their overall intensity changes and use them as the dissimilarity constraint in the SDC-based disc reconstruction. Several major factors that often affect the disc dissimilarity computation and the disc reconstruction have been considered, including BVs, uneven illumination within each disc image, and the illumination changes between different images. In addition, a sparsity constraint is also included in SDC inspired from the observation that a few reference disc images closest to the testing disc image are usually sufficient to estimate its CDR. The main contributions of this paper include

1) a novel SDC method for CDR assessment which considers both dissimilarity constraint and sparse constraint;

2) a new method to compute the dissimilarity between two disc images;

3) the results show that the proposed method achieves much more accurate CDR assessment and better glaucoma screening performance than the state-of-the-art methods.

Different from most of previous methods which are based on low-level image segmentation, this method computes an optimal sparse linear reconstruction of the input disc from the most similar reference discs to estimate the CDR. This makes the algorithms more robust to the cases where the contrast between optic cup and rim is low.

2 LITERATURE SURVEY

2.1 Optic Disk And Cup Boundary Detection Using Regional Information

The main visual clues used by clinicians to estimate the cup boundary from CFI are: a) change in color near pallor boundary and b) bend in small blood vessels. Hence, we make use of color information and structural properties of cup region to get the cup boundary. Having compared several color spaces, we found the cup region appears most continuous (except major vessel occlusion in nasal side) and well contrasted against the background in the *'a'* plane of the *Lab* color space. For further processing, we take *'a'* colour plane in which cup region appears dark. A morphological opening with a small circular element is carried out to smoothen small blood vessels present in the cup region. Then, we linearly transformed intensity values to the range of [0-1] and extract pixels using a dynamic threshold t to select only pixels which fall inside the OD region.

The intensity normalization step and the spatial constraint imposed on the extracted pixels (relevant pixels are always inside OD) make threshold selection trivial. We empirically select a value of $t = 0.07$ which perform consistently well on our dataset. We use the knowledge about the cup structure to divide the cup into a nasal cn and temporal ct regions.

2.2 Effects of Preprocessing Eye Fundus Images on Appearance Based Glaucoma Classification

Early detection of glaucoma is essential for preventing one of the most common causes of blindness. Our research is focused on a novel automated classification system based on image features from fundus photographs which does not depend on structure segmentation or prior expert knowledge. Our new data driven approach that needs no manual assistance achieves an accuracy of detecting glaucomatous retina fundus images comparable to human experts. In this paper, we study image preprocessing methods to provide better input for more reliable automated glaucoma detection. We reduce disease independent variations without removing information that discriminates between images of healthy and glaucomatous eyes.

Our method uses intensity information from the images as well as geometric assumptions on the width, length and structure of the vessels. We use an adaptive thresholding technique, wherein for each pixel, the median of its 15_15 neighborhood is taken as a threshold to separate foreground from background. The size of the neighborhood was determined to approximately match the size of the structures, i.e. the vessels.

2.3 Classifying Glaucoma with Image-based Features from Fundus Photographs

Glaucoma is one of the most common causes of blindness and it is becoming even more important considering the ageing society. Because healing of died retinal nerve fibers is not possible early detection and prevention is essential. Robust, automated mass-screening will help to extend the symptom-free life of affected patients. We devised a novel, automated, appearance based glaucoma classification system that does not depend on segmentation based measurements. Our purely data-driven approach is applicable in large-scale screening examinations.

Our system achieves 86% success rate on a data set containing a mixture of 200 real images of healthy and glaucomatous eyes. The performance of the system is comparable to human medical experts in detecting glaucomatous retina fundus images. We build a robust, automated glaucoma detection system using color fundus images in a data-driven way. Therefore, image-based features are provided that are new in the domain of glaucoma detection. This, so called appearance based approach is well-known from object and face recognition [13, 14]. The technique is based on statistical evaluation of the data and does not depend on explicit outlining of the optic disc, as required for global or sector-based shape analysis.

Consequently, preprocessing and image-based feature extraction has a major influence on the classification process. This work shows the influence of different image-based features on the accuracy of glaucoma classification from fundus images.

3 EXISTING SYSTEM

3.1 Brightness-Based Method

Glaucoma is one of the most common causes of blindness. It is induced by the progressive loss of retinal nerve fibers in the par papillary region. Lost fibers cannot be revitalized but the progression of the disease can be stopped [1]. For this reason, early detection of glaucoma is essential for affected patients. Diagnosis is commonly done by direct examination of the important neuroretinal rim [2] using an ophthalmoscope or based on digital retina images acquired by devices such as the Heidelberg Retina Tomography (HRT) [3] or the Kowa NonMyd fundus camera (Fig. 1). In this work, we use the modality of color fundus photographs.

In our approach, the feature extraction and classification is fully automated and is not segmentation dependent. This appearance based approach is well known from object and face recognition [7, 8]. It is a data driven technique based on statistical evaluation of the image data, e.g. by Principal Component Analysis (PCA). This promising approach is new in the field of retina imaging.

To provide a good basis for further investigations, we analyze the effect of normalizing the images by preprocessing methods on classification results. We show that reducing disease independent variations is possible without removing information that discriminates between healthy and glaucomatous eyes. On one hand, no uniform illumination is a general problem in retinal imaging. It is due to the small size of the objects and the complexity of the optic system (including both the camera and the eye) involved in the imaging process. Such in homogeneities have to be corrected. On the other hand, blood vessels in retina images seem to be a distracting feature when diagnosing glaucoma.
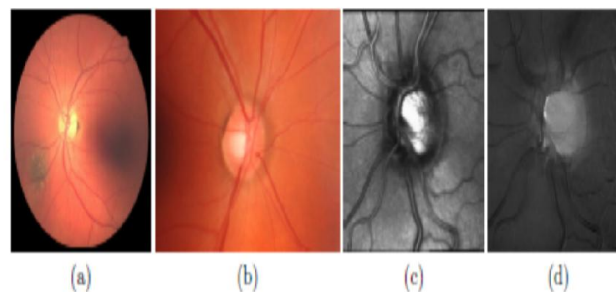
Figure 3.1:Example images of the eye ground: Color fundus photographs with large (a) and small fields of view (b), HRT reflectance (c) and topographic image (d).

3.2 Methods

As shown in the examples in Fig. 1, fundus images show important physiological structures of the eye ground, including the optic nerve head (ONH), the macula, and the blood vessels. Based on the usual practice in the clinic, we developed a scheme for automated processing and classification of the acquired images.
1. Correction of illumination and intensity in homogeneities,
2. In painting of the blood vessels,
3. Normalization of the region of interest for diagnosis,
4. Feature extraction,
5. Classification.

The focus of the work reported here is on the preprocessing steps (1-3). These are, however, essential for providing strong features and reliable classification. We show in this paper the effect of the preprocessing steps on glaucoma classification using a fixed configuration of feature extraction and

classifier. The features are computed by PCA, and then used in a Support Vector Machine (SVM) to classify the images. The obtained results are evaluated by comparing them with given diagnoses.

Inpainting of the Vessels Our method uses intensity information from the images as well as geometric assumptions on the width, length and structure of the vessels. We use an adaptive thresholding technique, wherein for each pixel, the median of its 15_15 neighborhood is taken as a threshold to separate foreground from background.

The region covered by the vessel mask is inpainted. It is an iterative technique, used in photo restoration and video processing [14, 15], that interpolates missing pixel values from those of the neighborhood in a visually pleasing way

3.3 Normalization of the ONH Region of Interest

We use papilla centered fundus photos for normalization. Previously proposed registration methods map images of the same subject [16] and mostly focus on vessel structures. Meaningful registration of fundus images of different subjects, however, is problematic and may not be feasible. Thus, we only apply a circular mapping of the neuroretinal rim.

The ONH appears in fundus images as an extremely bright, mostly circular region. We used a slightly modified version of the ONH localization method of [4]. It uses a mean filtering with a large kernel and threshold probing for rough localization, and then a circular Hough transform on the edge map to find the border of the neuroretinal rim.
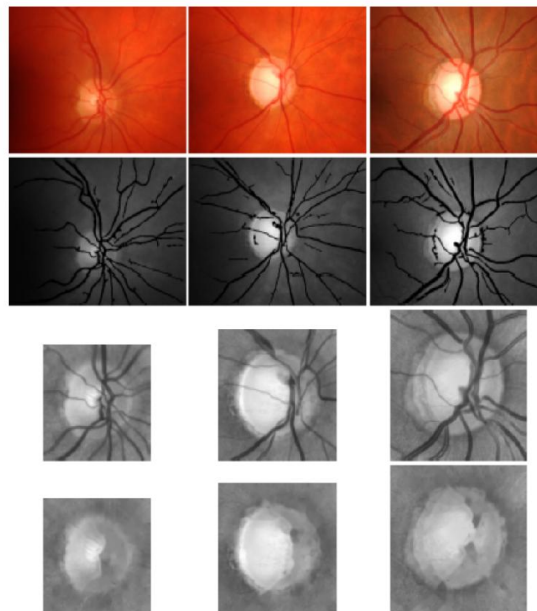
Figure 3.2:Preprocessed Images, row to row: Original fundus photos, vessel masks overlaid onto the green channel image, illumination corrected and cropped ROIs, image ROIs after inpainting. First column: a healthy retina; Second column: a glaucomatous optic disc; Third column: a healthy retina with macro papilla.

3.4 Evaluation

The objective of this work is to study the effect of preprocessing within the domain of automated glaucoma classification. Therefore, we evaluated different combinations of the above described methods with a fixed feature extraction technique and a fixed classifier. The ROIs were scaled (interpolated) to a fixed reference size of 128 _ 128 pixels and that was taken directly as a high dimensional feature vector. Dimensionality reduction was done by Principal Component Analysis (PCA) [8]. We took the first 30 components as features for classification. As a classifier, we selected the SVC type Support Vector Machine (SVM) [17] with penalization parameter 0:5, cost-parameter c = 1, using the radial basis kernel and normalized input data.

The images used in this study were acquired by a Kowa NonMyd alpha digital fundus camera with a papilla centered 20 field of view and an image size of 1600 X 1216 pixels (see first row of Fig. 2). For

evaluation, we took 200 images (50 images each of healthy and glaucomatous eyes for training and a similar mixture for separate testing; age of the subjects: 57_10 years) randomly selected from the Erlangen Glaucoma Registry (EGR).

4 PRPOSED SYSTEM

4.1 Disc Localization, Segmentation, and Normalization

In order to compute the CDR using the proposed SDC, it is important to locate and segment the disc. The disc localization focuses on finding an approximate location of the disc, very often the disc center. It has been extensively studied for applications in diabetic screening [21]. The disc localization is often achieved based on brightness [22], [23], anatomical structures among the disc, macula, and retinal BVs [24], [25] or the relative locations of these anatomical structures [26], [27]. In this paper, the disc is located using our earlier brightness-based method in [23], which works well in our datasets for glaucoma screening as there are few white lesions to confuse disc localization as compared to diabetic screening.

Many algorithms have been proposed for disc segmentation, such as template-based approaches [28], [29], deformable model-based approaches [6], [30] and classification-based approaches [5], [31]. In this paper, we segment the disc using the state-of-the art self-assessed disc segmentation method [32], which is a combination of three approaches.

4.2 Self-Assessed Disc Segmentation

Optic disc segmentation from retinal fundus image is a fundamental but important step in many applications such as automated glaucoma detection. Very often, one method might work well on many images but fail on some other images and it is difficult to have a single method or model to cover all scenarios. Therefore, it is important to combine results from several methods to minimize the risk of failure. The self-assessed disc segmentation proposed in [32] selects one result based on the outputs from three individual disc segmentation methods. Each individual method obtains a disc boundary and computes a self-assessment score that reflects a confidence or reliability of its automated result. The self-assessed method determines the disc by applying the three disc detection methods one by one until a confident output is obtained.

4.3 Disc Normalization

There are many choices for the disc representation. Earlier experience [5], [9], [17] shows that the green channel of the retinal color image is the most suitable one for CDR computation. Therefore, we use this channel in the paper. All disc images from right eyes are flipped horizontally to avoid the difference between the left and right eyes.
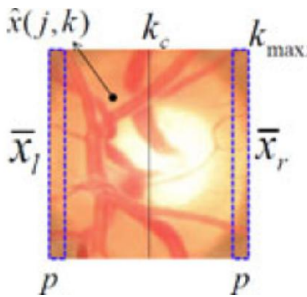
1) BV Removal: The BVs within the disc vary largely among different individuals. The disc reconstruction and the dissimilarity computation between two disc images are greatly affected by them. Therefore, it is important to remove the BVs. Many automated vessel detection methods [33], [34] reported in the literature can be used. In this application, we found it unnecessary to use very complex and time-consuming vessel segmentation to get precise BVs for the disc dissimilarity computation and later the disc reconstruction. Instead, an approximate segmentation of BV is sufficient for the objective of computing the disc dissimilarity. In this paper, we use a morphological closing process with an empirically selected structure element size of 5 to estimate the BV

$$BV(j,k) = \begin{cases} 1, & \text{If } |x(j,k) - \tilde{x}(j,k)| > T \\ 0, & \text{otherwise} \end{cases} \quad (1)$$

where $\tilde{x} = \text{morph}(x)$ denotes the image after applying a morphological closing process on x. Then, the vessel removed image
$\hat{x}$ is obtained by replacing the vessel pixels in x with the pixels
in $\tilde{x}$, i.e.,

$$\hat{x}(j,k) = \begin{cases} \bar{x}(j,k), & \text{If } BV(j,k) = 1 \\ x(j,k), & \text{Otherwise.} \end{cases} \qquad (2)$$


Figure 4.1:Illustration of unbalance correction: A linear mapping based on the average intensities on the left and right side.

2) Within Disc Uneven Illumination Correction: Uneven illumination across the optic disc is another factor that affects the dissimilarity computation and the disc reconstruction. Very often, the temporal side of the disc is brighter than the nasal side while the unbalance varies from one disc image to another. In our method, we apply a linear mapping to correct the unbalance. As shown in Fig. 2, we first compute the average intensity $\bar{x}l$ and $\bar{x}r$ from the first and last p columns of the disc $\hat{x}$. Then, the balance corrected disc xb is computed as

$$x_b(j,k) = \frac{(k - k_c)}{k_{max} - p}(\bar{x}_l - \bar{x}_r) + \hat{x}(j,k) \qquad (3)$$

where kc is the center column of the disc, and $k$max is the maximum number of columns. In this paper, we set p as 10% of $k$max, i.e., $p = 5$ for our disc resized to be 50×50. The performance of the method is not sensitive to the value of p.

4.4 Block Diagram
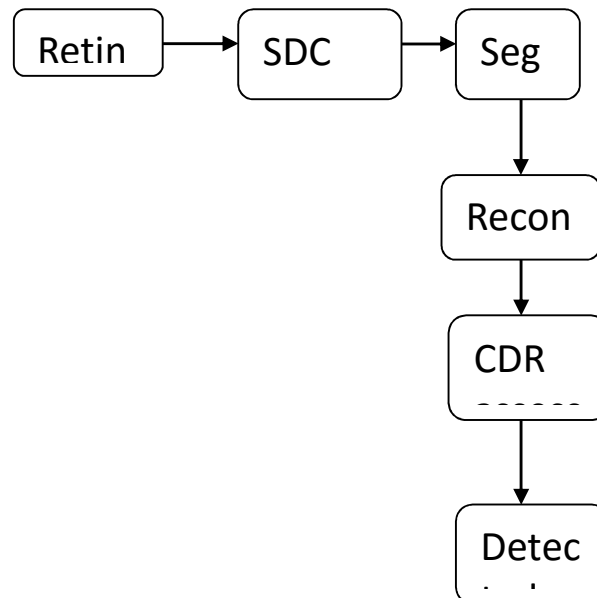
***Figure 4.2:Block Diagram***

4.4.1 Sparse Dissimilarity-Constrained Coding

In this section, we introduce the proposed spare dissimilarity constrained coding algorithm. Denote a set of n reference disc images $X = [x1, . . . , xn]$ and the corresponding CDRs as $r = [r1, r2, . . . , rn]T$, $i = 1, 2, . . . , n$, xi denotes the ith balance corrected disc computed above. Inspired from the reconstruction

based method [19], we want to compute a linear reconstruction coefficient $w = [w1, . . . , wn]T$ for a new testing disc image y while minimizing the reconstruction error $\_y - Xw\_2$. From our experience, a few reference disc images that are closest to y are sufficient to estimate the CDR for y while too many reference images often lead to a bias especially when the reference images do not have uniform CDR distribution. Therefore, we want to limit the number of reference images used, i.e., we want to minimize the nonzeros elements in w, or $\_w\_0$. Because $\_0$ - norm is a NP-hard problem, the $\_1$-norm $\_w\_1$ is used instead. In addition, as the reconstruction is more accurate from images more similar to the test disc, we add the difference between the reference and test disc images as a regularization term in the objective function to penalize the use of references.
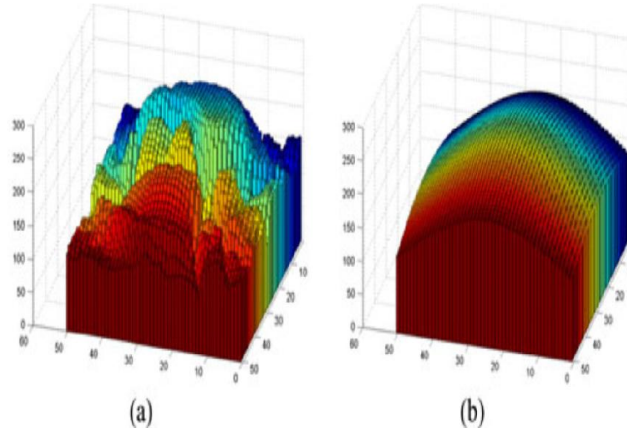
Figure 4.3:Illustration of surface fitting on a disc image. (a) A disc in 3-D plot. (b) Best-fitted disc surface.

4.4.2 Dissimilarity

It is important to compute a dissimilarity score between two discs which reflects their CDR difference. As mentioned, the previously used Gaussian distance [19] often suffers from noise, imperfect vessel removal, etc. Therefore, it faces some challenges to represent the actual CDR difference between two discs. Very often, we found two discs with similar CDRs have a Gaussian distance even larger than two discs with significant different CDRs. Therefore, Gaussian distance is not a good choice. In fact, this is also the reason that a *k*-nearest neighbor (kNN) approach works poorly for this task. In this paper, we observe that the overall intensity change within the disc is highly related with the CDR value. Motivated from this, we propose to apply surface fitting within the disc image to compute the dissimilarity.

4.4.3 Solution

The problem in (10) is a standard $\_1$ norm regularized leastsquare minimization problem. It has been shown that this unconstrained convex optimization problem can be represented as the following constrained optimization problem [35]

$$\underset{w}{\mathrm{argmin}} \left(\|\hat{y} - \hat{X}w\|^2 \right), s.t., \|w\|_1 < t$$

where t is inversely related to $\lambda 2$. It can be solved by least angle regression (LARS) [36].
In LARS [36], $\tilde{y} = X\tilde{}w$ is initialized with all zeros and iteratively updated. In each iteration, the feature most correlated with the objective function in (10) without $\_1$-norm penalty is selected and added into an active set Ω. $\tilde{}y$ is updated in the direction of most correlated feature until another feature with equivalent correlation is added. When there is more than one feature in Ω, LARS updates $\tilde{}y$ in a direction equiangular among all features. More details of the algorithms can be found in [36].

4.4.4 CDR Assessment

After solving (10), we obtain w. Then, the ratio $\hat{}r$ is computed as

$$\hat{r} = \frac{1}{1_w^T w} r^T w$$

where **1**w is a vector of 1s with length equals to the size of w.
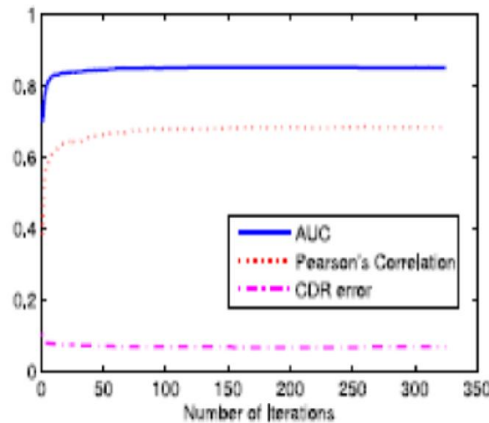In this paper, manual CDRs from the reference images are used to form r.

Figure 4.4:Accuracies after each LARS iteration.

4.4.5 Performance Evaluation Under Different Settings
        To evaluate the robustness of the proposed method, it is important to conduct the tests under different settings.
1) Parameters: There are two main parameters $\lambda 1$ and $\lambda 2$ in the SDC. The first parameter $\lambda 1$ determines the weight of the dissimilarity regularization. In this paper, we conduct a cross validation search in $10-10$, $10-9, \ldots , 1010$ in a reference set and we found that 104 gives best result.
2) Reference Images: The reference images used to reconstruct the discs are important. Since there are many possibilities to divide the SiMES images for reference and testing, it is important to know how different partitions affect the performance. In our tests, we conduct the tests with n from 25 to 325 with a step of 50. In the experiments, we obtain ten different random partitions and conduct twofold cross validation in each partition. Each partition divides the images to set Ai and Bi with 325 images in each set, $i = 1, 2, \ldots , 10$.
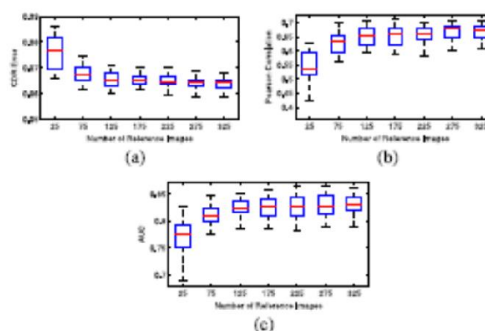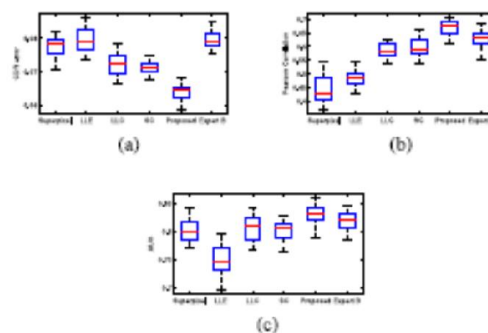

*Figure 4.5:Box plot of performance for different number of reference images. (a)
CDR Error. (b) Pearson's Correlation. (c) AUC.*

        It takes 0.17 to 4.0 s for a new disc image tested with 325 reference images when the number of iterations is changed from 100 to 300 using a dual core 3.0-GHz PC with 3.25-GB RAM. Since Fig. 4 shows that an iteration of 100 times is sufficient to obtain a stable result, we fix a maximum of 100 iterations for the rest of the tests. The number of reference images n affects the computational cost linearly.

4.5 Comparison With Other Methods

        To compare the proposed SDC method with other methods, we tested the two most competitive state-of-the-art methods using superpixel [18] and LLC [19]. Besides LLC, we have also implemented two other possible reconstruction-based approaches based on sparse coding (SC) [38] and locally linear embedding (LLE) [39] to justify the effectiveness of the regularization used in the proposed method.

Compared with other reconstruction-based methods such as SC [38] and LLE [39], the proposed method also achieves better results, which justifies the benefits of using the dissimilarity constraint and the sparsity constraint in SDC. The proposed method achieves an accuracy even better than the "Expert B."


Figure 4.6:Box plot of performance by different methods. (a) CDR error. (b) Pearson's Correlation. (c) AUC.

This implies that the method can be used for automated CDR computation without decreasing the accuracy compared with a manual one. Fig. 6 uses box plots to show the performance variations by different methods in the SiMES images. We have also conducted the *t*-test to evaluate the significance level of the difference between the proposed method and other methods including superpixel, LLE, SC, and LLC as well as manual CDRs by "Expert B."

4.6 Effect of Reference Manual CDRs

In the above, we have shown the results when we use the first set of manual CDRs from "Expert A" to form r in (12). Since manual assessment of CDRs is very subjective, it is reasonable that different people give different manual CDRs especially for challenging cases without obvious contrast between cup and rim. Therefore, it is important to evaluate how different r would affect the results. In this paper, we also use manual CDRs from "Expert B," as well as the average CDRs between "Expert A" and "Expert B" to form r in (12) and compute CDRs. Therefore, we obtain three sets of automated CDRs.

6 RESULTS
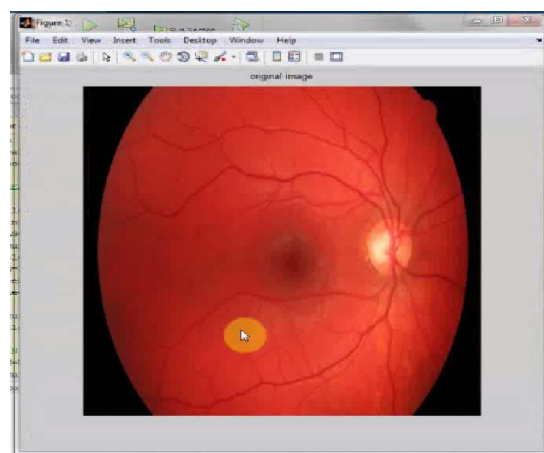
Figure 6.1: Original Image
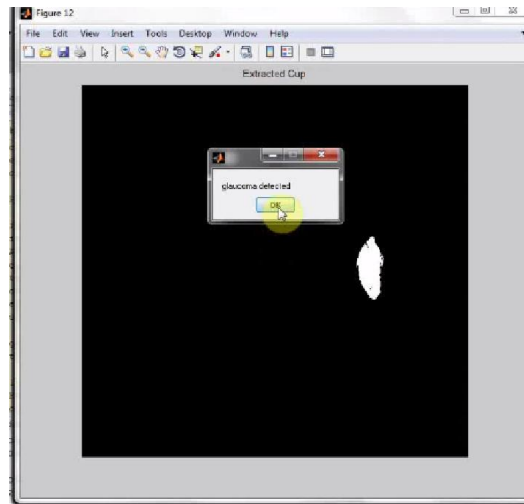
Figure 6.2: Output image

CONCLUSION AND FUTURE WORK

Compared with previous methods using superpixel or LLC, it improves the CDR computation accuracy by more than 10%. The previous bias of underestimating the large CDRs is reduced. Even though this is likely because the CDRs are computed based on the "Expert A" CDRs measured by the same person, it shows that the proposed method achieves an error smaller than the inter observer error. Therefore, the proposed method can be potentially used to replace manual CDR assessment to save time and reduce cost. The limitation is that the method may not capture local cup deformation. It is also interesting to note that by using average CDRs from the two sets of manual CDRs as reference and ground truth, the proposed method achieves smaller CDR error and higher correlation.

Future work will explore the integration of other factors to improve diagnostic outcomes toward a more reliable and efficient glaucoma screening system.

REFERENCES

[1] H. A. Quigley and A. T. Broman, "The number of people with glaucoma worldwide in 2010 and 2020," *Brit. J. Ophthalmol.*, vol. 90, no. 3, pp. 262–267, 2006.

[2] S. Y. Shen, "The prevalence and types of glaucoma in Malay people: The Singapore Malay eye study," *Investigative Ophthalmol. Vis. Sci.*, vol. 49, no. 9, pp. 3846–3851, 2008.

[3] P. J. Foster *et al.*, "The prevalence of glaucoma in Chinese residents of Singapore: A cross-sectional population survey of the Tanjong Pagar district," *Arch. Ophthalmol.*, vol. 118, no. 8, pp. 1105–1111, 2000.

[4] Centre for Eye Research Australia. (2008). Tunnel vision: The economic impact of primary open angle glaucoma. [Online]. Available: http://nla.gov.au/nla.arc-86954

[5] M. D. Abr`amoff *et al.*, "Automated segmentation of the optic disc from stereo color photographs using physiologically plausible features," *Investigative Ophthalmol. Vis. Sci.*, vol. 48, pp. 1665–1673, 2007.

[6] J. Xu *et al.*, "Optic disk feature extraction via modified deformable model
technique for glaucoma analysis," *Pattern Recognit.*, vol. 40, pp. 2063– 2076, 2007.

[7] Z. Hu *et al.*, "Automated segmentation of neural canal opening and optic cup in 3-D spectral optical coherence tomography volumes of the optic nerve head," *Investigative Ophthalmol. Vis. Sci.*, vol. 51, pp. 5708–5717, 2010.

[8] M. D. Abr`amoff *et al.*, "Automated segmentation of the cup and rim from
spectral domain OCT of the optic nerve head," *Investigative Ophthalmol. Vis. Sci.*, vol. 50, pp. 5778–5784, 2009.

[9] G. D. Joshi *et al.*, "Optic disk and cup segmentation from monocular color retinal images for glaucoma assessment," *IEEE Trans. Med. Imag.*, vol. 30, no. 6, pp. 1192–1205, Jun. 2011.

[10] J. Meier *et al.*, "Effects of preprocessing eye fundus images on appearance based glaucoma classification," in *Proc. 12th Int. Conf. Comput. Anal. Images Patterns*, 2007, pp. 165–172.
Proc. Int. Conf. Image Process., 2001, vol. 2, pp. 837–840.